Current - voltage characteristics of the resonant tunnelling double-barrier structure under time-periodical perturbation

1996 J. Phys.: Condens. Matter 8 8869

(http://iopscience.iop.org/0953-8984/8/45/020)

J. Phys.: Condens. Matter **8** (1996) 8869–8887. Printed in the UK

Current–voltage characteristics of the resonant tunnelling double-barrier structure under time-periodical perturbation

Evgeny N Bulgakov and Almas F Sadreev

Kirensky Institute of Physics, 660036, Krasnoyarsk, Russia

Received 22 January 1996, in final form 4 July 1996

Abstract. We consider a typical semiconductor resonant tunnelling GaAs/AlGaAs/GaAs nanostructure which forms a double-barrier potential with quasienergy levels corresponding to transition frequencies in the infrared and microwave regions. Two types of dynamical perturbation of the heterostructure in the form $V_1(x,t) = V_1 x \cos \Omega t$ and $V_2(t) = V_2 \cos \Omega t$ are considered. We analyse numerically a reconstruction of the electron transmission through the heterostructure and the current–voltage characteristics (IVC) under the influence of these dynamical perturbations. Both weak and strong perturbations are considered. We investigate the dependences of the transmission on the electron energy and the frequency of the external field with the main accent on the case where a frequency of the perturbation is tuned to a transition between quasienergies of the double-barrier structure. It is found that these resonant phenomena give rise to new peaks and dips in the IVC. In particular, it is shown that the dipole type of perturbation $V_1(x,t)$ gives rise to a Rabi splitting of the transmission peaks and under certain conditions to a Rabi splitting of the IVC peaks and dips. We demonstrate that dynamical perturbation may induce a direct current opposite to the direction of the applied voltage, and that this phenomenon takes the form of a sharp dip which has a resonant origin. It is observed that the dipole type of perturbation $V_1(x,t)$ of laser radiation is more effective for tuning the IVC than the first perturbation $V_2(t)$. Also absorption and emission of energy by an electron transmitted through the DBRTS are considered.

1. Introduction

One significant manifestation of quantum effects in mesoscopic systems is the resonant tunnelling that takes place in a heterojunction nanostructure, fabricated from semiconductor materials such as GaAs/$Al_xGa_{1-x}As$ and consisting of artificial potential barriers and quantum wells with dimensions of the order of the electron wavelength. Since the pioneering work of Tsu and Esaki [1], and Chang, Esaki, and Tsu [2], there has been a great deal of interest, both experimental and theoretical, in double-barrier resonant tunnelling structures (DBRTS). The most common DBRTS experiments involve application of a bias across the device while measuring the resulting current. The typical DBRTS current–voltage characteristic (IVC) has one or more differential negative-resistance regions depending on the well width. Because the IVC is the most readily measured quantity, we focus here on its calculation with the aim of investigating how dynamical processes in DBRTS induced by time-periodical perturbations are reflected in the IVC.

Over the past decade resonant tunnelling through a time-modulated potential has attracted considerable interest. Inspired by the original Büttiker and Landauer [3] (see

0953-8984/96/458869+19$19.50

also Haavig and Reifenberger [4]) study of a single time-modulated barrier, significant recent theoretical interest has focused on quantum tunnelling in a variety of time-dependent potentials. The main issues in this area include: exact solutions for the transmission probability for various forms of the potential barriers [5, 6]; the time of tunnelling [7–9]; and 'elevator resonance activation' of tunnelling particles by an adiabatically varying potential [10]. In application to the DBRTS the first study [11] of the resonant tunnelling through the DBRTS in the presence of a harmonic time-dependent potential was based on a model in which the static potential barriers and the harmonic time-dependent potential were both taken to be δ-functions. Jauho and Jonson [12, 13, 14], Cai *et al* [15, 16], Jiang [17] and Wagner [18] investigated the photon-assisted transmission of an electron through the DBRTS with the potential barriers and well chosen in the rectangular form. In [13] the DBRTS was considered for time modulation of both the potential barriers and the potential well. The numerical results derived by Jauho [13] demonstrate different peculiarities of the transmission probability depending on parameters of the system. That is, it was shown that the satellite peaks in the transmission probabilities correspond to the absorption/emission of modulation quanta. It was also pointed out that the time-periodical modulation of the potential well influences the transmission probability more significantly than the time-periodical modulation of the potential barrier. Complete destruction of the photon-assisted resonant tunnelling in the form of strong quenching of the transmission probability was found by Wagner [19] for certain amplitudes and frequencies of the time-periodical perturbation $V_2 \cos \omega t$ acting on the central well in the DBRTS.

The work of Sollner *et al* [20] began experimental studies of the effect of time-dependent potentials in resonant tunnelling through semiconductor microstructures. They studied the influence of electromagnetic radiation on the resonant tunnelling current. Much later experimental investigations of the tunnel current through the DBRTS under the influence of far-infrared radiation modulation were presented by Chitta *et al* [21–23]. In [23] the changes in the current density due to the radiation, as a function of the dc bias voltage, were measured for different frequencies of the radiation. Theoretically the changes in the tunnel current through the DBRTS, which we—following Chitta *et al*—will call the FIR response, were considered by Chitta *et al* [21] and Dakhnovskii and Metiu [24]. Also note references [25–27] where the time-dependent tunnel current was considered as a response to an external time-dependent voltage. Although these studies use different models of the electron tunnelling through the DBRTS, the time-dependent perturbation inside the DBRTS was considered as spatially uniform in the well.

However, as well as the dc electric field, E_0 gives rise to a coordinate-dependent perturbation of the form eE_0x, and the irradiated electric field may have coordinate dependence. To be specific, we assume that the laser beam is parallel to the layers of the heterostructure. If the polarization of the time-dependent electric field is directed along the electron transmission direction (i.e. perpendicular to the DBRTS layers), the time-dependent perturbation will take a similar form, namely $eE_1x \cos \omega t$. This dipole type of perturbation is easier to exploit experimentally than the type that is spatially uniform in the well. Because it is of dipole type, this dynamical perturbation should mix different quasilocalized states in the quantum well and to lead to a Rabi splitting, as occurs in atomic systems [28]. It would give rise to a Rabi splitting of the resonant transmission. This phenomenon was first demonstrated by Johansson and Wendin [29]; it was what they called the dynamical Stark effect in the two-level approximation for the quantum well obtained with the help of a Green's function treatment. The coherent and sequential tunnelling through the DBRTS assisted by electromagnetic radiation with the wave vector parallel to the DBRTS and polarized in the direction of electron transport was also considered by Iñarrea *et al* [30].

However, they restricted consideration to just the first-order time-dependent perturbation theory and were interested in problems where a quasilocalized resonant tunnelling state is coupled by the radiation with a continuum of states in the collector where the frequency of the radiation is much less than the difference between the quasienergies.

What seems to us especially interesting is that these perturbations may provide the possibility of experimentally observing resonant and nonlinear dynamical phenomena accessed up to now only in atomic and molecular systems. In fact, we demonstrate in the present work the resonant effects and the Rabi splitting of the resonant transmission which under certain conditions can be observed in the IVC provided that the frequency of time-dependent perturbation is tuned to the distance between the resonant tunnelling states of the DBRTS. The GaAs/AlGaAs/GaAs nanostructures are expected to provide perspective in the study of nonlinear dynamical perturbations because dipole matrix elements are enhanced in comparison with those in atomic systems, where they are restricted to the value ea where a is the Bohr radius.

2. Formulation of the model

As was considered in the introduction, suppose that the laser beam (i.e. its wave vector) is parallel to the interface of the heterostructure, and that the polarization of its electric component $\boldsymbol{E}(t) = \boldsymbol{E}_1 \cos \Omega t$ is directed normal to the interface—i.e., is directed along the x-axis, which is the direction of the electron transmission. The radiation field is spatially uniform over the whole heterostructure including the electrodes and potential barriers. However, as was shown by Jauho [13], the effect of the radiation in the barriers is much less strong than that in the potential well. This is quite clear if we take into account the fact that the eigenfunctions corresponding to the quasienergy levels of the DBRTS are exponentially small over the barriers. For the electrodes we—following [29]—assume that the frequency of the radiation exceeds the plasma frequency ($\approx$40 meV) of the electron gas in the doped electrodes. Therefore most of the absorption/emission of radiation by the tunnelling electrons occurs when they are in the quantum well.

Since there is no electrostatic field parallel to the interface of the heterostructure, the problem of the electron transmission is reduced to solving a one-dimensional Schrödinger equation of the form

$$\mathrm{i}\hbar \frac{\partial \psi(x,t)}{\partial t} = \left\{ -\frac{\hbar^2}{2m^*}\frac{\partial^2}{\partial x^2} + U(x) - eE_0 x + eE_1 x \cos \Omega t \right\} \psi(x,t) \qquad (1)$$

where the potential $U(x)$ creates a double-barrier form in the x-direction while in the y- and z-directions we have free motion. In reality, although in these directions the sample is restricted, we can consider the electron system as a two-dimensional electron gas (2DEG). And in any case we may separate space variables.

There is another case—that of polarization parallel to the interface of the DBRTS. Such an alternating electric field mixes different transverse (evanescent) states of the 2D electron gas described by a wave vector parallel to the layers of the DBRTS, $\boldsymbol{k}_\parallel$. Taking into account the fact that the wavenumber of the FIR photons is much less than the wavenumber of the electrons with $k_F \sim 10^5$ cm^{-1}, the radiation will produce almost vertical transitions of electrons (presumably Γ–Γ points of the electron band). In that case the dynamical perturbation can be written as

$$V(t) = E_1 \langle \boldsymbol{k}_\parallel | d | \boldsymbol{k}'_\parallel \rangle \cos \Omega t = V_2 \cos \Omega t.$$

Therefore that perturbation can be considered as spatially uniform in the quantum well of the DBRTS.

It is convenient in what follows to introduce the dimensionless variables

$$\xi = x/x_c \qquad \tau = t/t_c \qquad \bar{a} = a/x_c \qquad \bar{b} = b/x_c \tag{2}$$

$$\omega = \frac{\hbar\Omega}{V_c} \qquad \Lambda = \frac{eE_1 b}{V_c} \qquad \lambda = \frac{V_2}{V_c} \qquad \gamma = \frac{\lambda}{\omega} = \frac{V_2}{\hbar\Omega} \tag{3}$$

where

$$t_c \equiv \frac{\hbar}{V_c} \qquad x_c \equiv \frac{\hbar}{\sqrt{2m^* V_c}}$$

where a is the barrier thickness, b is the quantum well width, and V_c is the characteristic dimensional constant which will be chosen below in the numerical calculations to be equal to the potential barrier height V_b (approximately a few hundreds of meV). Moreover, the characteristic length x_c is comparable with the width of the potential well. In the dimensionless variables, equation (1) takes the following form:

$$\mathrm{i}\frac{\partial\psi(\xi,\tau)}{\partial\tau} = \left[-\frac{\partial^2}{\partial\xi^2} + u(\xi) - v_0\xi + \Lambda\frac{\xi}{\bar{b}}\cos\omega\tau\right]\psi(\xi,\tau) \tag{4}$$

where the dimensionless 1D potential of the heterostructure is $u(\xi)$, and $v_0 = eE_0x_c/V_c$. For the case of a time-dependent perturbation that is spatially uniform in the quantum well the coupling term takes the form $\lambda\cos\omega\tau$.

3. Transmission and reflection amplitudes

As was discussed in the introduction, the coherent radiation has its main effect inside the quantum well of the DBRTS. Hence, we can assume that the time-periodical perturbation takes place in the potential well only. Following [3, 4] we write the wave function as follows:

$$\psi(\xi,\tau) = \sum_{n=-\infty}^{\infty} \exp[-\mathrm{i}(\epsilon + n\omega)\tau]\psi_n(\xi) \qquad \epsilon = E/V_c$$

and substitute it into equation (4). Then integration over all times gives inside the well

$$(\epsilon + n\omega)\psi_n(\xi) = -\frac{\partial^2\psi_n}{\partial\xi^2} + \frac{\Lambda}{2\bar{b}}\xi\left[\psi_{n-1} + \psi_{n+1}\right] - v_0\xi\psi_n. \tag{5}$$

Following [3, 4] we write the wave function of the left electrode in the following form:

$$\psi_L(\xi,\tau) = \mathrm{e}^{-\mathrm{i}\epsilon\tau + \mathrm{i}k_0\xi} + \sum_{n=-\infty}^{\infty}\psi_{n,L}\mathrm{e}^{-\mathrm{i}k_{n,L}\xi - \mathrm{i}\epsilon\tau - \mathrm{i}n\omega\tau} \tag{6}$$

and the wave function of the right electrode as

$$\psi_R(\xi,\tau) = \sum_{n=-\infty}^{\infty}\psi_{n,R}\mathrm{e}^{\mathrm{i}k_{n,R}\xi - \mathrm{i}\epsilon\tau - \mathrm{i}n\omega\tau} \tag{7}$$

where

$$k_{n,R}^2 = \epsilon + n\omega + v_0\bar{b} \qquad k_{n,L}^2 = \epsilon + n\omega. \tag{8}$$

In the framework of the chosen scheme of the time-dependent perturbation, equation (5) is exact, and a solution of it will be found numerically with the appropriate number of channels to provide sufficient exactness of the calculations. Specifically, we find all amplitudes $\psi_n(\xi)$, including the amplitudes of the right and left electrodes $\psi_{n,R}$ and $\psi_{n,L}$.

4. Numerical results on the transmission probabilities

We introduce the transmission probability of the nth satellite channel T_n as

$$T_n = \frac{\mathrm{Re}(k_{n,R})}{k_{0,L}}|\psi_{n,R}|^2. \tag{9}$$

The transmission probability T_n defines a probability that an electron injected at the left-hand electrode with energy ϵ will be at the right-hand electrode with energy $\epsilon + n\omega$. This means that during transmission through the DBRTS the electron will absorb/emit n quanta of the external field. The accuracy of the computation was controlled by the requirement that

$$\sum_n [T_n(\epsilon, \omega) + R_n(\epsilon, \omega)] = 1$$

where

$$R_n(\epsilon, \omega) = \frac{\mathrm{Re}(k_{n,L})}{k_{0,L}}|\psi_{n,L}|^2$$

is the reflection probability in the nth channel. Generally, the function T_n depends on both ω and ϵ.

To find the probabilities T_n it is necessary to solve the infinite system of equations (5). Actually, the numerical calculations show that the values T_n converge rapidly to zero when $n \to \infty$, and for $|n| > n_c$ the transmission probabilities T_n are negligible. The domain of convergence $|n| < n_c$ essentially depends on the perturbation parameter Λ/ω. We find that n_c is roughly proportional to the value of the perturbation parameter: at $\Lambda/\omega = 2.5$, $n_c \approx 2$; at $\Lambda/\omega = 7.5$, $n_c \approx 7$.

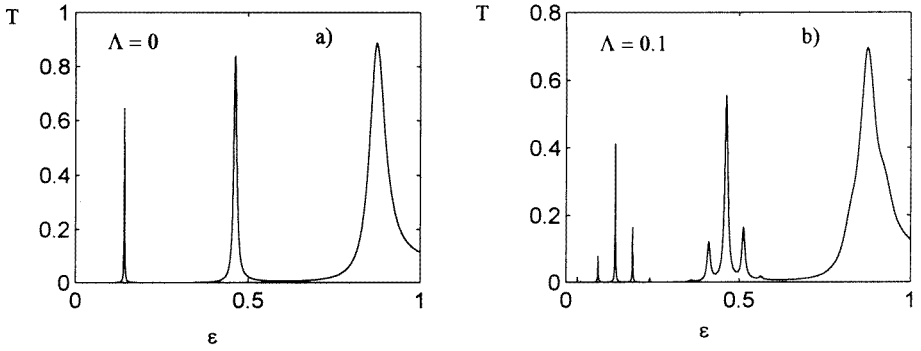

Figure 1. The dependence of the total transmission probability $T(\epsilon)$ on the dimensionless energy ϵ of an injected electron in the DBRTS under the influence of the dipole-type time-periodical perturbation $V(\xi, \tau) = \Lambda\xi \cos\omega\tau$ for the nonresonant case. The dimensionless bias $\phi = v_0\bar{b} = 0.256$ and the frequency of the time-periodical field $\omega = 0.05$. The parameters of the DBRTS are chosen as follows: $v_b = 1, \bar{a} = 3.0, \bar{b} = 10$. Three resonant peaks correspond to the second and third quasienergies in the potential well: $\epsilon_2 - \phi/2 = 0.1365$, $\epsilon_3 - \phi/2 = 0.4665$.

Using the rapid convergence of the functions T_n, we calculated numerically the dependence of the total transmission probability $T(\epsilon, \omega)$:

$$T(\epsilon, \omega) = \sum_{n=-n_c}^{n_c} T_n(\epsilon, \omega). \tag{10}$$

We performed the following calculations of the function $T(\epsilon, \omega)$: the dependence on ϵ at fixed ω (we denote that function as $T(\epsilon)$), and the dependence on ω at fixed energy ϵ (we denote this function as $T(\omega)$) for the specific parameters $v_b = V_b/V_c = 1$, $\bar{a} = 3$, $\bar{b} = 10$. The first equality means that for a characteristic energy V_c a height of barrier V_b was chosen. It is useful to rewrite these specifications in dimensional units. For a concentration of Al in the barriers of $x = 0.33$, the conduction band offset is equal to $V_b = 245$ meV [31]. For this concentration, tunnelling through the $Al_xGa_{1-x}As$ barrier proceeds exclusively through the Γ–Γ minima [32] of the electron band. Moreover we consider that the radiation does not involve indirect X–Γ transitions because the wavelength of the radiation far exceeds $2\pi/k_F$. Taking into account a simple empirical relation for the electron mass [33], $m(x) = m(1 + \alpha x)$ where $m \approx 0.066m_0, \alpha \approx 0.895$, we obtain $x_c = 12.8$ Å, $a = 38.4$ Å, $b = 128$ Å. For these parameters of the DBRTS, the maxima of the stationary transmission are for the following values of the energy of the incident electron (quasienergy levels):

$$\epsilon_1 = 0.068\,16 \qquad \epsilon_2 = 0.269\,12 \qquad \epsilon_3 = 0.5899$$

or in dimensional units

$$E_1 = 16.7 \text{ meV} \qquad E_2 = 65.93 \text{ meV} \qquad E_3 = 144.53 \text{ meV}.$$

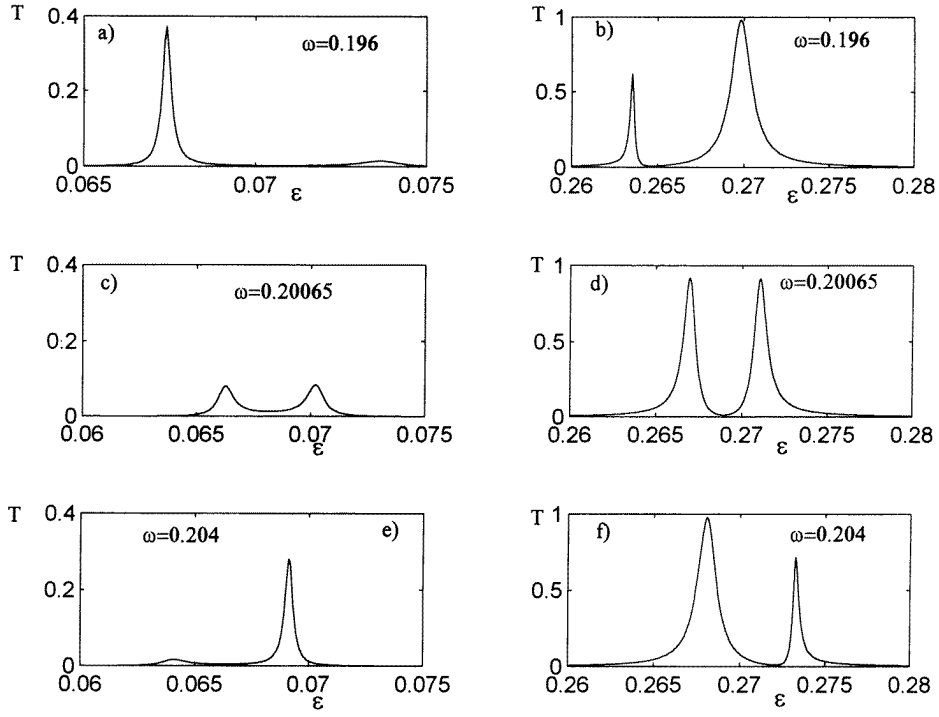

Figure 2. The Rabi splitting of the first and second resonant transmission peaks shown in figure 1 for the case of resonant dipole perturbation. The dipole matrix element $\xi_{12} \approx 0.18$. The external bias is switched off. The parameters of the DBRTS are the same as in figure 1.

The dependence of the transmission probability $T(\epsilon)$ on the energy, when the external electric ac field and the time-periodical spatially uniform perturbation are both switched

on, was calculated in [12, 13, 15–17, 23, 34]. The results are that the modulation of the potential well by weak perturbations gives rise to two additional resonant peaks located at the energies $\epsilon_1 \pm \omega$. Also two slight photon-assisted peaks were obtained by Iñarrea *et al* [30] via perturbation theory for the time-periodical perturbation $\boldsymbol{p}\mathbf{A}(t)$. These peaks are demonstrated in figure 1. Thus for the nonresonant perturbation there is no principal difference between the spatially uniform time-dependent effects and the spatially uniform effect of dipole type. Increasing of the perturbation parameter $\gamma = \lambda/\omega$ leads to the appearance of new transmission channels at the quasienergies $\epsilon_i \pm n\omega$ and to the strong suppression of the initial channels with quasienergies ϵ_i. In particular Wagner [18, 19] found the dependence of the transmission probability as a function of the amplitude and frequency of the spatially uniform time-dependent perturbation, and discovered strong quenching of the transmission probability due to zeros of the Bessel functions. However, for a resonant case, such as that of the dipole interaction of the DBRTS with radiation mixing the quasienergy levels, we may expect resonant effects which are well known in atomic and molecular systems coupled with the radiation. Among them is the Rabi splitting of the resonant peaks of the transmission by a frequency

$$\Omega_r^2 = \left(\frac{\epsilon_i - \epsilon_j - \omega}{2}\right)^2 + \Lambda^2 |\langle i|\xi|j\rangle|^2 \tag{11}$$

where $\langle i|\xi|j\rangle = \xi_{ij}$ is a matrix element of the dipole transition between quasienergy states i and j. The corresponding new positions of the resonant tunnelling through the DBRTS are

$$\tilde{\epsilon}_{i,j} = \frac{\epsilon_i + \epsilon_j}{2} \pm \Omega_r. \tag{12}$$

These formulae are easily obtained in the two-level approximation [28].

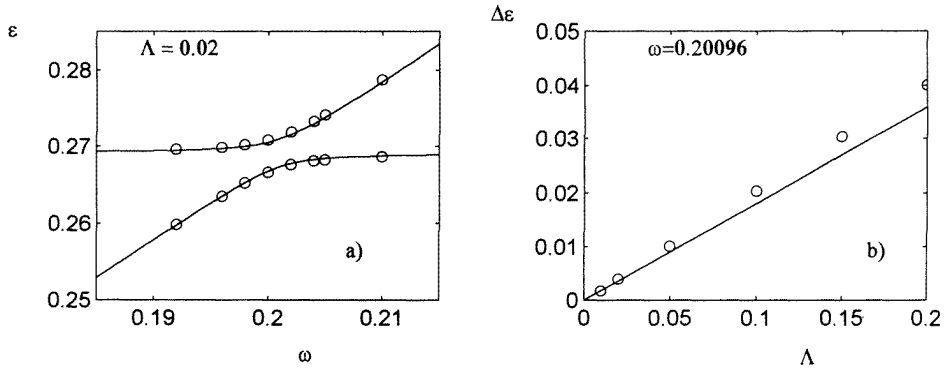

Figure 3. (a) The frequency dependence of the Rabi splitting calculated (circles) and defined by formula (12) (continuous curves). (b) The linear dependence of the Rabi splitting $\Delta\epsilon$ on the coupling constant Λ for the case defined in figure 2.

The Rabi splitting of peaks of the resonant tunnelling through the DBRTS under the influence of resonant time-periodical dipole perturbation is demonstrated in figure 2. Figures 2(a) and 2(b) show the case where the frequency of the radiation is slightly below $\epsilon_2 - \epsilon_1$; figures 2(c) and 2(d) correspond to the exact resonant perturbation $\omega = \epsilon_2 - \epsilon_1$, and figures 2(e) and 2(f) show the case where the frequency of the radiation is slightly above

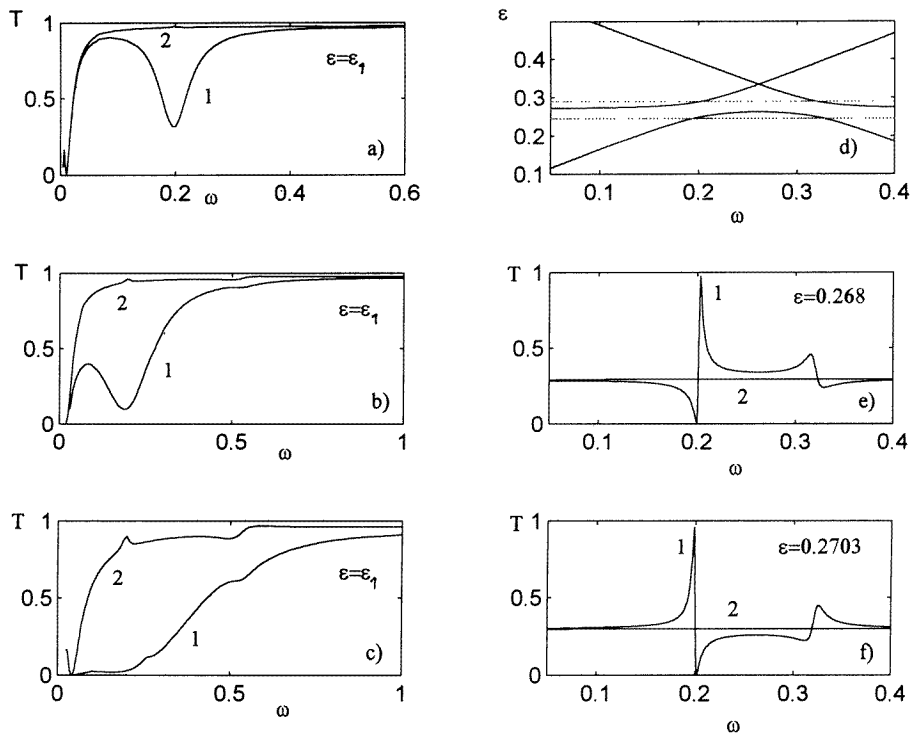

Figure 4. The frequency dependences of the total transmission probability for the dipole perturbation $\Lambda\xi\cos\omega\tau$ (curves 1) and the time-periodical perturbation spatially uniform in the quantum well $\lambda\cos\omega\tau$ (curves 2) when the energy of the incident electron is resonant with the first quasienergy of the DBRTS. (a) $\lambda = 0.025$, $\Lambda = 0.05$; (b) $\lambda = 0.05$, $\Lambda = 0.1$; (c) $\lambda = 0.1$, $\Lambda = 0.2$. (d) A schematic view of the frequency behaviour of the energy levels described by formulae (11) and (12). (e) and (f) show the cases where the energy of the incident electron is slightly above and below the quasienergy ϵ_2 shown in (d) by dashed lines; $\lambda = 0.025$, $\Lambda = 0.05$. The parameters of the DBRTS are as follows: $\bar{a} = 3.0$, $\bar{b} = 10$, $v_b = 1$, $\phi = 0$.

$\epsilon_2 - \epsilon_1$. Qualitatively these pictures of the Rabi splitting coincide with those obtained by Johansson and Wendin [29]. In figure 3 the Rabi splitting of the second peak of the resonant tunnelling through the DBRTS as a function of the frequency (a) and amplitude (b) of radiation is plotted as circles. It is compared with formulae (11) and (12), and demonstrates excellent agreement. A small deviation between the the calculated Rabi splitting and the splitting from formula (12) in figure 3(b) is explained by the fact that there is a shift of quasienergy levels in the second order of perturbation.

A substantial difference between the dipole type of time-periodical perturbation and the spatially uniform perturbation is seen for the energy of the incident electron tuned to the quasienergy level of the DBRTS, as is shown in figures 4(a), 4(b) and 4(c). The external bias is switched off for simplicity. The most interesting frequency behaviour of the total transmission is observed when the energy of the incident electrons slightly deviates from the quasienergy level, as is shown in figures 4(e) and 4(f). This deviation should be less than the width of the quasienergy level. In an effort to understand this unusual frequency behaviour we show schematically in figure 4(d) the Rabi splittings of energies with increasing frequency. For a deviation $|\epsilon - \epsilon_2|$ less than the width of the second

quasienergy level ϵ_2 for small frequency, the transmission is almost constant and exceeds zero. In the vicinity of the first resonance defined by the relation $\epsilon_1 + \omega = \epsilon_2$, the first Rabi splitting takes place. It leads to a deviation of the quasienergy level $\tilde{\epsilon}_2$ up from the energy of the incident electron with a consequent decrease of the transmission. Increasing of the frequency leads to intersection of the first quasienergy level $\tilde{\epsilon}_1$ with the energy of the incident electron, with a corresponding sharp increase and decrease of the transmission. Further increasing of the frequency gives rise to a new Rabi splitting with the quasienergies $\epsilon_1 + \omega$ and $\epsilon_3 - \omega$. This pattern is repeated in the opposite sequence except as regards the heights and widths of the peaks, because of the different widths of the quasienergy levels ϵ_i of the DBRTS. If the energy of the incident electron was tuned to slightly above ϵ_2, the pattern would be repeated in the opposite way, as is shown in figure 4(f).

While the dipole time-periodical perturbation $\Lambda\xi \cos\omega\tau$ gives rise to essential features of the frequency dependences of the total transmission probability, as is seen from figure 4(a), 4(b) and 4(c) (curves 1), the spatially uniform perturbation $\lambda \cos\omega\tau$ has no visible peculiarities except slight peaks at resonant frequencies for strong-coupling constants (curves 2). Huge resonant dips shown by curves 1 are easily explained by the Rabi splitting (see figure 3(a)). Slight peaks induced by spatially uniform time-periodical perturbation are just satellite peaks located at $\omega = \epsilon_2 - \epsilon_1$. Thus, the radiation field in the infrared region coupled with the DBRTS provides the possibility of strongly governing the resonant tunnelling near resonance. As will be shown in the next section, the same is true for the IVC.

5. The current–voltage characteristics driven by external time-periodical perturbations

One of the most important characteristics of the DBRTS is their extremely fast electric response which has been demonstrated in their application as detectors up to 2.5 THz [20] and quantum well oscillators up to 420 GHz [35]. Chitta *et al* [23] investigated both theoretically and experimentally the influence of far-infrared radiation on the tunnel current of the DBRTS. In order to couple the radiation to the confined electrons inside the quantum well, they used a grating coupler geometry to obtain a component of the ac electric field from the radiation perpendicular to the layers (parallel to the current). This scheme provides a coupling of the DBRTS with the radiation field via the term $\boldsymbol{p}\mathbf{A}(t)$ (or, equivalently, via the dipole-type interaction), so the calculations of Iñarrea *et al* [30] were able to give good agreement with the experiments of Chitta *et al*.

In this section we consider the current–voltage characteristics under the influence of the spatially uniform time-periodical perturbation $\lambda \cos\omega\tau$ and the dipole one $\Lambda\xi \cos\omega\tau$ with the aim of investigating resonant phenomena in the IVC. The first case of the perturbation was considered by Chitta *et al* [23], who showed substantial changes of the IVC peak, and Dakhnovskii and Metiu [24], who were the first to demonstrate a negative direct current opposite to the direction of the applied voltage. Here we only complement these investigations by consideration of the IVC for stronger couplings and a wider range of the bias.

The effects of the dipole type of time-periodical electric fields on the IVC were considered by Johansson and Wendin [29] and Iñarrea *et al* [30]. For the resonant case of the time-periodical perturbation the dynamic Stark shift of the first IVC peak was demonstrated [29]. In a related section, we aim to demonstrate the Rabi splitting of the IVC and consider conditions under which that phenomenon can be observed.

Formulae for the current induced by constant bias may be found in various references

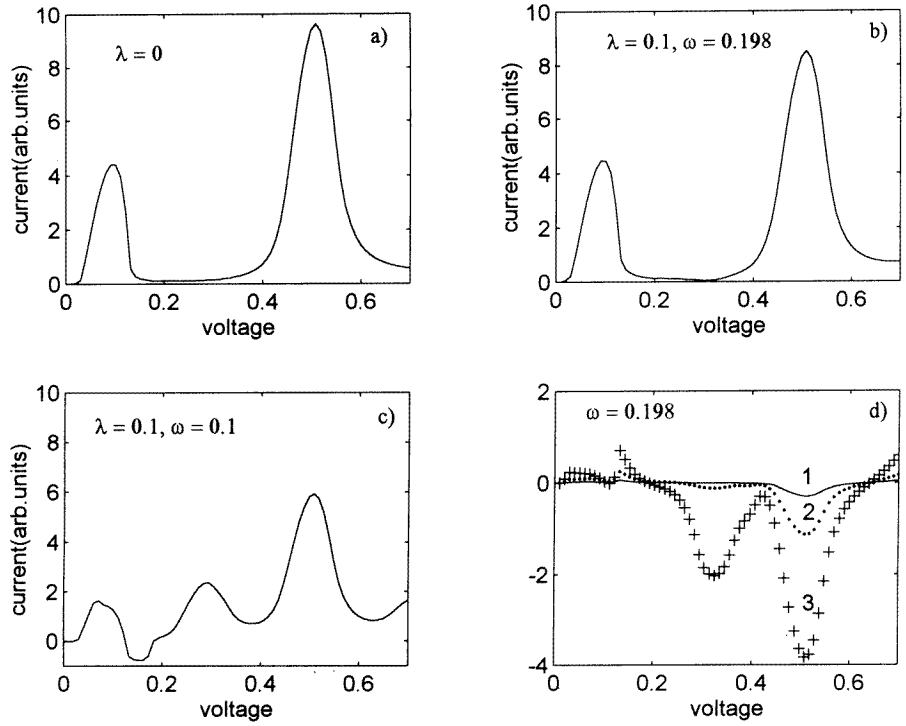

Figure 5. Current–voltage characteristics of the DBRTS under the influence of the spatially uniform time-periodical field $\lambda \cos \omega\tau$. (a) The static case is shown with two peaks corresponding to the first and second quasienergies. (b) The frequency of the ac field is resonant with the quasienergy levels: $\omega = \epsilon_2 - \epsilon_1 = 0.198$ (7.76×10^{13} Hz). (c) The perturbation parameter $\lambda/\omega = 1$. (d) The difference between the stationary IVC and the IVC affected by the ac field, where the continuous curve (1) corresponds to $\lambda = 0.05$, the dotted curve (2) corresponds to $\lambda = 0.1$, and '+' (3) corresponds to $\lambda = 0.2$. The conduction band width of the electrodes is equal to 0.05 (12.25 meV). The arbitrary unit of current corresponds to 777.5 A cm^{-2} and the unit of the external constant voltage corresponds to 0.245 V provided that the concentration of Al in the barrier layers is equal to 0.33. It is seen from (c) and (d) that moderate dynamical perturbation leads to a negative peak of the current for positive voltage. The parameters of the DBRTS are chosen as follows: $\bar{a} = 1.5, \bar{b} = 10$ Å ($a = 19.2$ Å, $b = 128$ Å).

(see, for example [32, 30, 36]). Here we use the following expression for the total current:

$$I_L = \frac{4em^*V_c^2}{\hbar^3}\frac{1}{(2\pi)^2}\int_0^{\sqrt{\epsilon_F}}(\epsilon_F - k^2)k(T_{L,R} - T_{R,L})(\epsilon)\ \mathrm{d}k \tag{13}$$

where $T_{L,R}, T_{R,L}$ are the total probability of transmission from left to right and from right to left defined by formula (10). They interchange for negative bias ϕ.

5.1. The IVC of the DBRTS under the influence of the spatially uniform time-periodical perturbation

Obviously, one can expect in accordance with figure 4 that for this perturbation there are no visible resonant effects in the IVC. In figure 5 the IVC are shown: for the static case (a); for the case of resonant perturbation with frequency $\omega = \epsilon_2 - \epsilon_1$ (b); and for the

nonresonant case (c). Comparison of figures 5(a) and 5(b) shows that an application of the resonant spatially uniform time-periodical perturbation has no effect. And only for rather small frequency when the perturbation parameter λ/ω is becoming of the order of unity can we see noticeable modifications of the IVC. Note that in figure 5 and forthcoming figures the current is presented in arbitrary units. In accordance with formula (13), if we choose the parameters of the DBRTS as in the previous section the unit of current density would correspond to a value of 777.5 A cm^{-2} and the unit of the external constant voltage would correspond to 0.245 V.

Strong spatially uniform time-periodical perturbation, as seen from figure 5(c), gives rise to an additional peak of the IVC at the voltage $\phi \approx 0.2$. Taking into account that the application of a bias approximately shifts the quasienergy levels in the DBRTS by the value $\phi/2$, one can easily recognize that this new peak is caused by a satellite peak of the total transmission.

The next peculiarity of the IVC is the appearance of a negative current for strong perturbation, as is seen from figure 5(c). This means that the ac electric field applied to the DBRTS forces current to flow in the direction opposite to the bias. The induced negative conductance was found firstly by Frishman and Gurvitz [37] in multiple-well heterostructures and then by Dakhnovskii and Metiu [24] in the DBRTS.

It is easy to understand this phenomenon if one takes into account the fact that the Fermi energy of both the right and the left electrodes is less than the frequency of the ac field. In computer simulations of the IVC the Fermi energy of the electrodes was chosen to be equal to 0.05 (12.25 meV), while the dimensionless frequency of the alternating fields is not less than 0.1. So, under increasing bias the satellite resonant channels approximately defined by the formula $\epsilon_i + n\omega - \phi/2$ may be beyond the conduction band of the left-hand electrode while these resonant channels may lie in the conduction band of the right-hand electrode lifted by the bias. Hence, this will give rise to a suppression of the left-hand current while the right-hand current will flow through the DBRTS.

In figure 5(d), like Chitta *et al* [23] we plotted the difference $\Delta I = I_{stat} - I_{dyn}$ (the FIR response) as a function of the bias. Qualitatively, features of ΔI for the first peak of the IVC are very similar to the ones calculated by Chitta *et al* with the assumption of spatially uniform time-periodical electric fields for the bias from zero to 0.2 which in dimensional units corresponds to a voltage of 50 mV. In the next region of bias, from 0.2 to 0.7 (from 50 mV to 172 mV), we can see stronger changes of the IVC under the effect of the spatially uniform time-periodical perturbation, and correspondingly we have huge differences ΔI near the second peak of the IVC. Obviously, the reason for that is that the second resonant quasienergy level ϵ_2 has a width of level substantially exceeding the width of the first quasienergy level ϵ_1.

5.2. The IVC of the DBRTS under the influence of the dipole time-periodical perturbation

As was seen from figures 2 and 4, the dipole time-periodical perturbation has a more substantial resonant effect on the transmission of electrons through the DBRTS in comparison with the spatially uniform one. It is reasonable to assume that the same is true for the IVC of the DBRTS, as is demonstrated in the following figures. In figure 6 the IVCs are shown for various coupling constants Λ and frequencies in the vicinity of the first resonance $\omega \approx \epsilon_2 - \epsilon_1$. As was mentioned in the introduction, the nonresonant effect of the dipole time-periodical perturbation was numerically considered by Iñarrea *et al* [30] and Wagner [19].

One can see from figure 6, even for a small coupling constant Λ, that the dipole

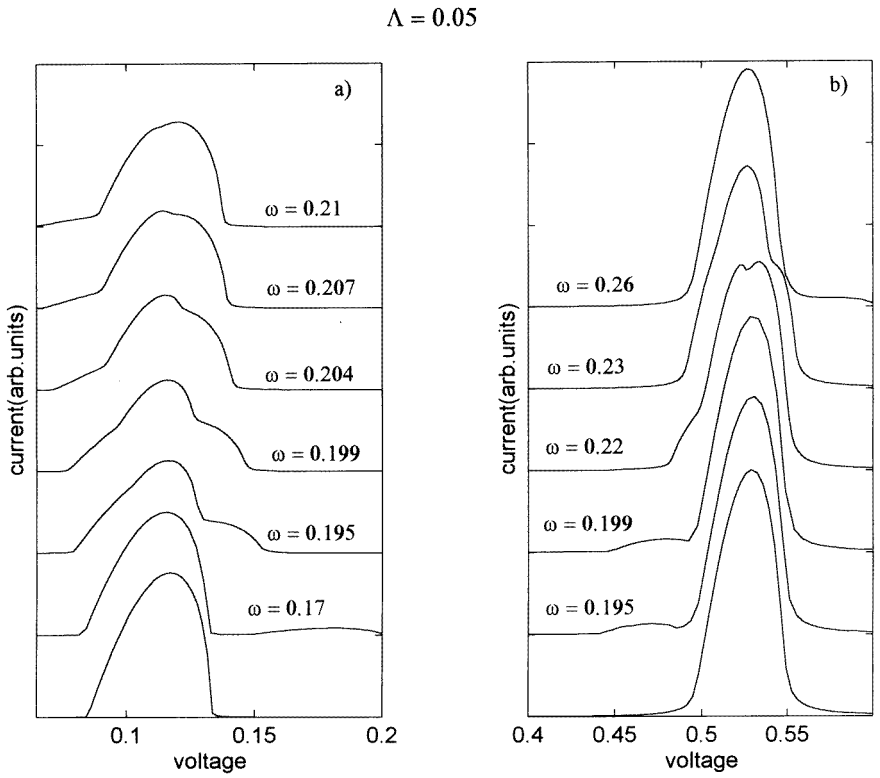

Figure 6. Current–voltage characteristics of the DBRTS under the influence of the dipole time-periodical perturbation $\Lambda\xi\cos\omega\tau$ with frequencies in the vicinity of the resonance $\epsilon_2-\epsilon_1=0.2$. The Rabi splitting of the first peak (a) and the second peak (b) of the IVC. The conduction band width of the electrodes is equal to 0.025. The lowest curve responds to the static case where $\Lambda=0$.

dynamical perturbation induces very noticeable changes of IVC peaks. Because of the resonance, the changes of the IVC reflect the Rabi splitting of the resonant transmission through the DBRTS. That effect is distinctly seen for a stronger coupling constant as is shown in figure 7. In both figures the evolution of the first and second peaks of the IVC with increasing frequency of the dynamical perturbation is shown. In correspondence with figure 2(a) one can see in figures 6 and 7(a) that the first stationary peak of the IVC for a frequency below the resonant one acquires a slight but wide additional peak at the right, which is increasing and approaching the left. For the resonant frequency of the dipole time-periodical perturbation we can see a splitting of peaks of the IVC. However, for the small coupling constant $\Lambda=0.05$ (figure 6) these peaks are strongly overlapped. For a frequency above the resonance we can see a small peak of the IVC at the left and a large peak at the right. Also, in full correspondence with figure 2(b), we can observe from figures 6 and 7(b) opposite evolution of the stationary second peak of the IVC related to the second quasienergy level of the DBRTS. These figures show that the IVC are very sensitive to the tuning of the frequency of the time-periodical electric fields to the energy differences between the quasienergy levels in the quantum well of the DBRTS. Moreover, to clearly observe the Rabi splitting of the IVC effected by the radiation field it is necessary to apply

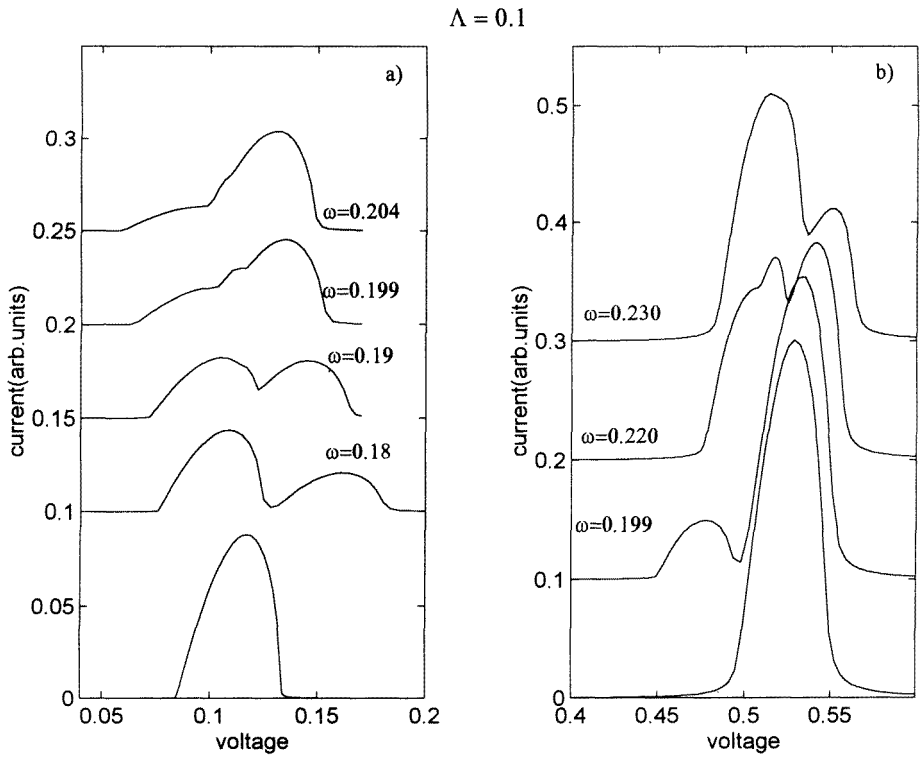

Figure 7. The same as in figure 6, but for a stronger coupling constant.

strong laser fields. However, in order to observe such a nonlinear optical phenomenon as the Rabi splitting of the IVC, the density of free carriers in the electrodes may have to be decreased. The width of the conduction band of the electrodes defined by the density of the free electrons (or holes) has the most importance for observing resonant phenomena in the IVC. This is shown in figure 8 for an extremely narrow conduction band of the electrodes equal to 0.01. Moreover one can observe the Rabi splitting not only of the basic stationary peaks of the IVC but even of a dip, as is shown in figure 8(c). The origin of the resonant two-photon dip is shown in figure 9. Assume that the conduction band of the left-hand electrode with the chemical potential μ_L does not coincide with any of the quasienergy levels of the DBRTS. Also assume that the splitting takes place for n-photon absorbed left-hand electrons with energy $\mu_L + n\omega$. Under these assumptions the transmission from the left to the right is prohibited ($T_{LR} = 0$ in formula (13)). On the other hand, assume that for n-photon absorbed right-hand electrons a condition

$$\mu_R = \mu_L - \phi \approx \tilde{\epsilon}_i - \phi/2 \tag{14}$$

is satisfied where the $\tilde{\epsilon}_i$ are the quasienergies of the DBRTS. For simplicity, the shift of the quasienergies inside the DBRTS induced by the bias ϕ was taken as $-\phi/2$ [32]. For the nonresonant time-periodical perturbation, $\tilde{\epsilon}_i \approx \epsilon_i + n\omega$ where n is an integer, while for the resonant effect, these quasienergies are given by (12). Relation (14) defines the position of a dip in the IVC. If we choose the frequency of the time-periodical perturbation equal to 0.14, in accordance with formula (14), we find that the two-photon resonant dip appears at

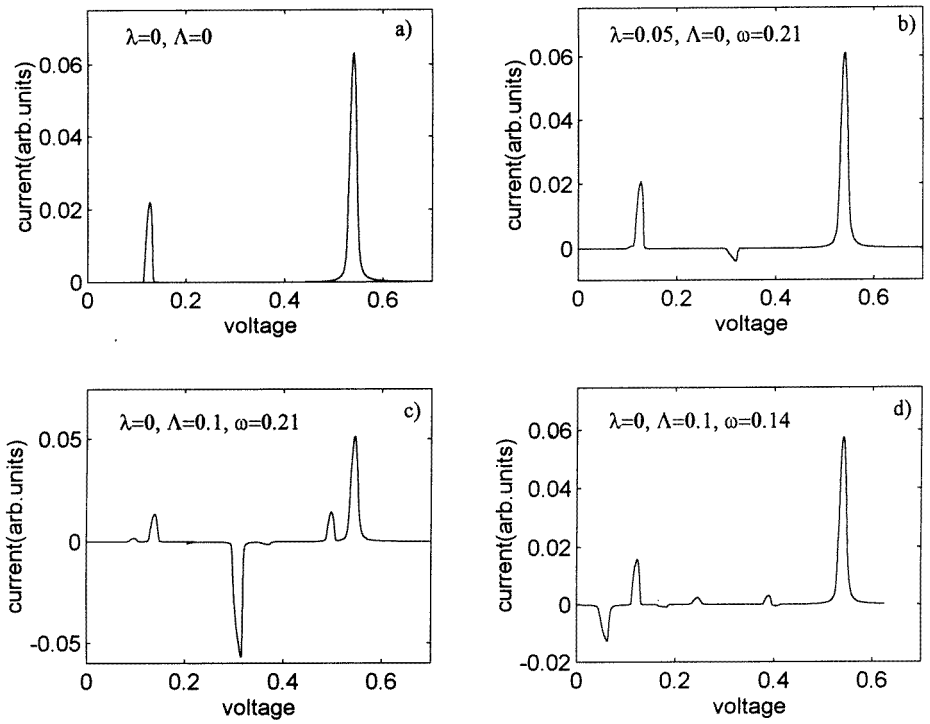

Figure 8. The IVC for an extremely narrow conduction band of the electrodes equal to 0.01, which demonstrates the Rabi splittings of the dip in the IVC. (a) The static case. (b) The spatially uniform time-periodical perturbation $\lambda \cos \omega\tau$ with a frequency resonant with $\epsilon_2 - \epsilon_1$. It is shown that there are no resonant effects for the dipole perturbation (c). (d) The case of the nonresonant dipole time-periodical perturbation which demonstrates that the position of the dip in the IVC is defined by two-photon excitation of electrons in the left-hand electrode at a voltage of $\phi = 2(2\omega - \epsilon_2)$.

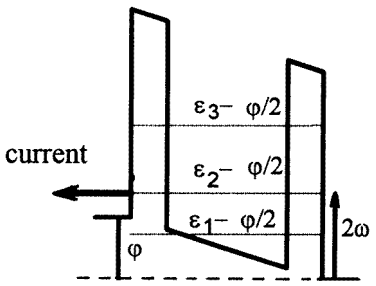

Figure 9. An illustration of two-photon excitation of the transmission from right to left.

the voltage $\phi_d \approx 2(2\omega - \epsilon_2) \approx 0.04$. In fact, the position of the resonant dip in figure 8(d) coincides with that estimate.

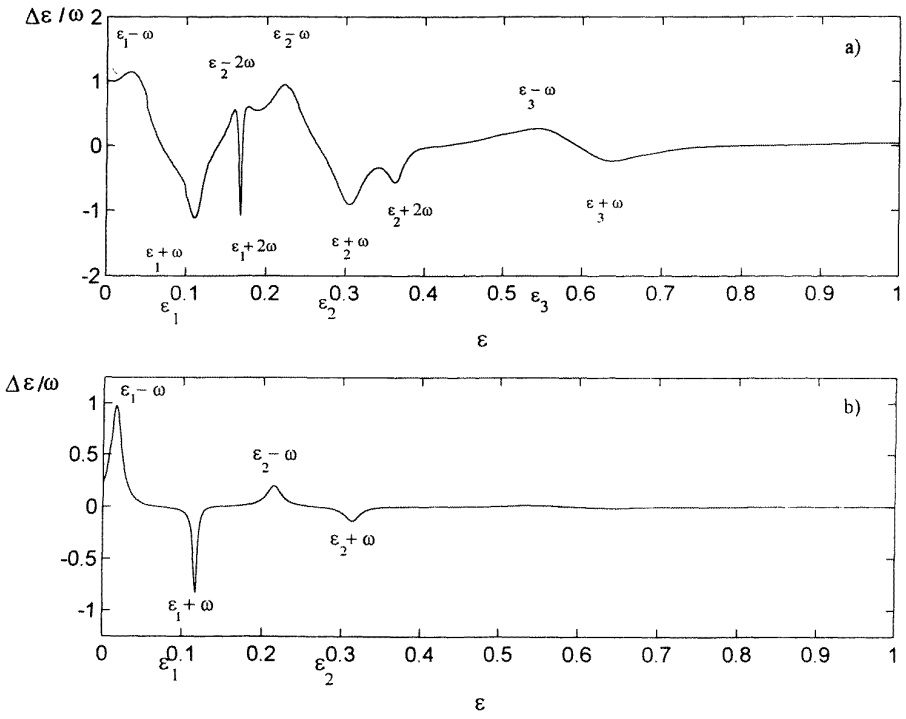

Figure 10. The dependence of the absorbed/emitted energy of an electron transmitted through the DBRTS, $\Delta\epsilon$, on the energy ϵ of an injected electron for a fixed value of the frequency $\omega = 0.05$ and for different values of the coupling constant λ. Arrows indicate the peaks of the resonances of absorption and emission of the modulation quanta; (a) $\lambda = 0.05$; (b) $\lambda = 0.01$.

6. Absorption and emission of energy by a transmitted electron

The transmission probability $T(\epsilon)$ has a resonant structure with peaks located at $\epsilon = \epsilon_i + n\omega$. This assumes that the transmitted electron may have an energy different from the energy of the injected electron due to the absorption or emission of the modulation quanta $n\omega$ [11, 12, 13]. For a small and moderate perturbation parameter $\gamma = \lambda/\omega$ the processes of absorption and emission of one modulation quantum dominate. In this section we will consider the energy absorbed/emitted by an injected electron transmitted through the DBRTS analytically and numerically for the case of a time-periodical perturbation spatially uniform in the quantum well.

The mean energy of the transmitted electron can be written as

$$\langle\epsilon\rangle = \int \psi_R^*(\xi,\tau)(-\partial^2/\partial\xi^2)\psi_R(\xi,\tau)\,\mathrm{d}\xi \Big/ \int |\psi_R(\xi,\tau)|^2\,\mathrm{d}\xi \tag{15}$$

where the integration is performed over the region of the right-hand electrode. After substitution of the wave function ψ_R defined by equation (7) into (15) and averaging over time we obtain

$$\Delta\epsilon \equiv \langle\epsilon\rangle - \epsilon = \sum_n n\omega t_n \Big/ \sum_n t_n. \tag{16}$$

where we have introduced the definition

$$t_n = |\psi_{n,R}|^2.$$

The function $\Delta\epsilon$ introduced in (16) describes the absorption ($\Delta\epsilon > 0$) or emission ($\Delta\epsilon < 0$) of energy by an electron transmitted through the DBRTS. This function was computed numerically. In figure 10 we present the dependence of the function $\Delta\epsilon$ on the energy of an injected electron ϵ. As figure 10 shows, for the energy of the injected electron tuned to $\epsilon_i - |n|\omega$, absorption of the modulation quanta takes place. For the energy of the injected electron tuned to $\epsilon_i + |n|\omega$, the emission of the modulation quanta occurs. When the energy of an injected electron is tuned to the fundamental resonant energies ϵ_i, the processes of absorption/emission of the modulation quanta by an electron are strongly suppressed. Figure 10(a) corresponds to moderate perturbation ($\gamma = 1$). In this case the processes of absorption/emission of one and two modulation quanta are easily seen.

The case of the small perturbation parameter $\gamma = \lambda/\omega \ll 1$ is shown in figure 10(b) for $\gamma = 0.2$. One can see that there are only the processes of the absorption/emission of one modulation quantum at energies equal to $\epsilon \pm \omega$. For $\gamma \ll 1$ the processes of absorption/emission of the modulation quanta can be investigated analytically on the basis of the perturbation theory. Consider, for example, the case where the energy of an injected electron is tuned to the 'left satellite': $\epsilon \approx \epsilon_i - \omega$, where $i = 1, 2, 3$. For $\gamma \ll 1$ we shall keep in the formulae the 0th channel ($m = 0$) since it gives the contribution to the transmission probability of the order γ^0, and the first channel with $m = 1$. Strictly speaking we should keep in the formula also the (-1)th channel (with $m = -1$) too. However the first channel is special because of its resonant denominator. Details of the calculations are given in [38]. Here we give only the final result for the absorption of energy by an injected electron which takes the following form:

$$\frac{\Delta\epsilon}{\omega} = \frac{t_1(\epsilon)}{t_0(\epsilon) + t_1(\epsilon)} \approx \frac{(\gamma/2)^2 r(\epsilon) r(\epsilon + \omega)}{1 + (\epsilon - \epsilon_i + \omega/\delta_i)^2} \tag{17}$$

where

$$r(\epsilon) = \frac{\sinh^2(\sqrt{1-\epsilon}\bar{a})}{4\epsilon\sqrt{1-\epsilon}}$$

and

$$\delta_i = \frac{\sqrt{\epsilon}}{\bar{b} r(\epsilon)}$$

is the width of the ith resonant quasienergy level. We can see that the expression (17) has a resonant structure at energies equal to $\epsilon_i - \omega$ which are observable in the numerical calculations presented in figure 10(b). Moreover, the values of $1/r(\epsilon)$ have the meaning of the probabilities of transmission through a single potential barrier. Hence, the less the degree to which the barrier is penetrable (the narrower the peak of the resonant tunnelling in the DBRTS), the more the effect of the resonant absorption of the energy.

We introduce the parameter $\lambda_c^{(i)}$ which characterizes (in the frames of the perturbation theory) the transition to the regime of saturation of the one-photon absorption for the transmission of an electron with the energy $\epsilon \approx \epsilon_i - \omega$ through the DBRTS. To estimate γ_c we use the condition $t_1(\epsilon) \sim t_0(\epsilon)$ which gives

$$\gamma_c^{(i)} \approx \frac{8\epsilon_i\sqrt{1-\epsilon_i}}{\sinh^2[\bar{a}\sqrt{(1-\epsilon_i)}]} \tag{18}$$

provided that $r(\epsilon) \approx r(\epsilon + \omega)$. The last condition simply means that $\omega \ll \epsilon$.

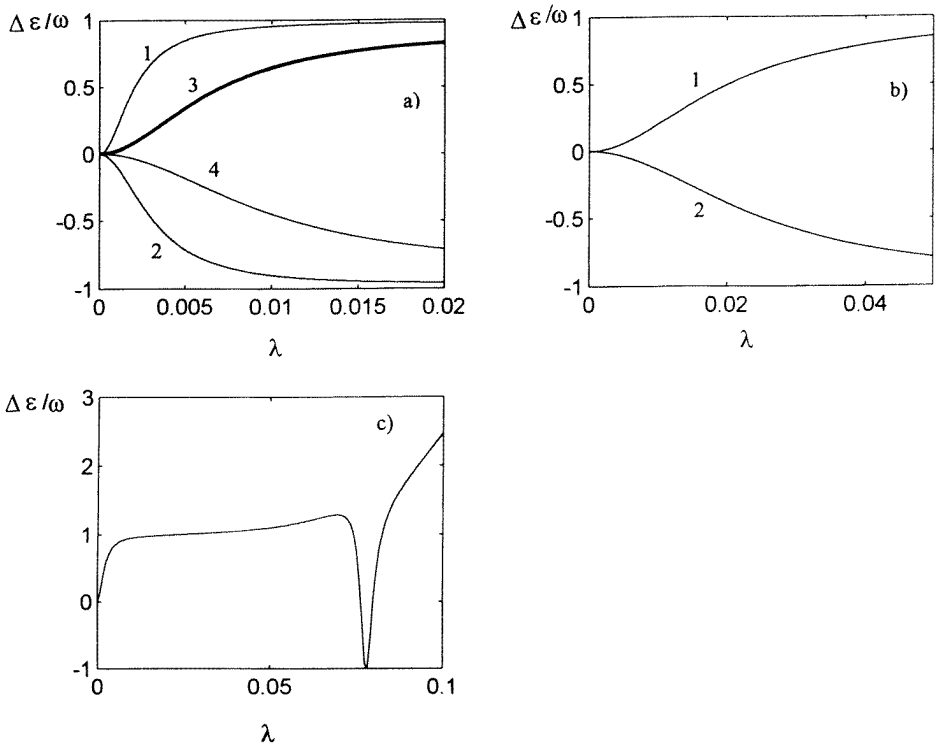

Figure 11. The dependence of the absorbed/emitted energy $\Delta\epsilon$ of the transmitted electron on the coupling constant λ. (a) Curve 1 corresponds to $\epsilon = \epsilon_1 - \omega$; curve 2 corresponds to $\epsilon = \epsilon_1 + \omega$; curve 3 corresponds to $\epsilon = \epsilon_1 - \omega - \delta$; curve 4 corresponds to $\epsilon = \epsilon_1 + \omega - \delta$ where $\delta = 0.004$ is the detuning from the resonance, and $\epsilon_1 = 0.066, \omega = 0.02$. (b) Curve 1 corresponds to $\epsilon = \epsilon_2 - \omega$; curve 2 corresponds to $\epsilon = \epsilon_2 + \omega$ where $\epsilon_2 = 0.2645, \omega = 0.05$. (c) The same as (a) but for larger values of the coupling constant λ.

The parameter $\gamma_c^{(i)}$ characterizes the crossover in the behaviour of the energy absorption $\Delta\epsilon$ to the perturbation parameter γ. That is, for $1 > \gamma > \gamma_c^{(i)}$ a transmitted electron absorbs approximately one modulation quantum, and the process of absorption is saturated.

Analogously, the perturbation theory (for $\gamma \ll 1$) can be developed for the right-hand satellites with $\epsilon \approx \epsilon_i + \omega$. In this case the main contributions to the transmission of an electron through the DBRTS give the 0, (-1)th channels. Thereby, for this case the processes are mainly those of emission of the modulation quantum.

In figure 11 we present the dependence of the absorbed/emitted energy $\Delta\epsilon$ of a transmitted electron on the coupling constant λ at the fixed values of ω obtained numerically. The curves 1 and 2 in figures 11(a) and 11(b) correspond to the energy of an injected electron tuned to the left-hand and the right-hand satellites, correspondingly. As one can see from figures 11(a) and 11(b) the curves have quadratic behaviour at small γ in agreement with formula (17) for the perturbation theory. When γ (or λ) is increased the curves change their behaviour, and the saturation takes place for the processes of absorption/emission of the energy. According to formula (18) we can find an estimation for $\gamma_c^{(i)}$. For the parameters chosen in figure 11(a), $\gamma_c^{(i)} \approx 0.1$, and for the parameters chosen in figure 11(b) $\gamma_c^{(i)} \approx 0.7$. As one can see these estimates are in good agreement with the results of the numerical

calculations presented in figures 11(a) and 11(b). When the energy of an injected electron is detuned from the exact resonance, the dependence of $\Delta\epsilon$ on γ (or λ) changes (see curves 3 and 4 in figure 11(a)), and becomes much weaker. When γ (or λ) increases significantly, the dependence of $\Delta\epsilon$ becomes more complicated; this is connected with the violation of the perturbation theory. In this case new channels appear in the transmission probability, which give the contribution to the behaviour of the absorption/emission of the electron's energy (see figure 11(c)).

7. Conclusion

The periodical modulation of the potential well with the frequency Ω in a double-barrier resonant tunnelling nanostructure leads to the appearance of additional channels in the transmission probability at the quasienergies $E_i + n\hbar\Omega$, where the E_i are the quasienergies of the unperturbed system. The dependences of the transmission probability on the energy of an injected electron and on the frequency of the external modulation field show that the resonant behaviour depends strongly on the perturbation parameters. We considered two types of perturbation: (a) a dipole time-periodical perturbation directed along the DBRTS which has the form $V_1(x, t) = V_1 x \cos \Omega t$; and for comparison (b) a spatially uniform time-periodical perturbation in the form $V_2(t) = V_2 \cos \Omega t$; these are both supposed to be localized inside the quantum well.

As was shown in figures 5–8, sufficient changes of the IVC in the form of substantial suppression of the stationary CVC peaks and the arising of new peaks and dips in the IVC take place for the dimensionless coupling constant Λ not exceeding 0.1 and for frequencies resonant with the differences between the quasienergies in the potential well. These frequencies have the order of 0.2. The main effect is the Rabi splitting of the stationary basic peaks of the IVC. The narrower the conduction band, the stronger the Rabi splitting (figures 7 and 8). The second effect is the Rabi splitting of the resonant dip shown in figure 8(c) which is caused by the two-photon processes shown in figure 9. Thus, measurements of the IVC may be used to observe resonant phenomena which take place for a frequency of the dipole type of the time-periodical perturbation near the distance between the quasienergies of the DBRTS. On the other hand, numerical calculations show that the time-dependent perturbation spatially uniform in the quantum well give rise to very weak resonant effects. Hence, the semiconductor heterostructures may be rather useful in the study of various resonant and nonlinear optical phenomena inherent in atomic systems.

If we restore the dimensional parameters of the DBRTS (the size of the well $b \approx 130$ Å, the height of the barrier $V_b = 245$ meV, and the frequency of the radiation $\Omega \sim 10^{13}$ Hz), the value of the dimensionless coupling constant $\Lambda = 0.1$ corresponds to the characteristic amplitude of the time-periodical electric field:

$$E_1 = \frac{2V_b\Lambda}{eb} \approx 4 \times 10^4 \text{ V cm}^{-1}. \tag{19}$$

Correspondingly, the power of the infrared laser should be more than $W \approx 4 \times 10^5$ W cm^{-2} with account taken of the coupling efficiency. Referring to Chitta *et al* [23] who used a FIR laser with a power of about 10 W, we see that this power of the laser is more than enough if we estimate the minimal square of the FIR laser beam as the length of the radiation wave in the square ($\sim 6 \times 10^{-6}$ cm^2). One can see from formula (19) that the dimensional amplitude of the radiation may decrease with the increasing of the width of the quantum well of the DBRTS and the decreasing of the height of the potential barriers.

Acknowledgments

We acknowledge fruitful discussions with David K Campbell (Illinois University, Urbana–Champaign). Most valuable discussions with Mathias Wagner (Hitachi Cambridge Laboratory) and Antti-Pekka Jauho (Mikroelectronik Centret, Technical University of Denmark) are gratefully acknowledged. Also we are very grateful to both referees for critical comments. This work was supported by the INTAS-RFFI Grant 657 i96 and the Krasnoyarsk Regional Science Foundation Grant 5F0060.

References

[1] Tsu R and Esaki L 1973 *Appl. Phys. Lett.* **22** 562
[2] Chang L L, Esaki L and Tsu R 1974 *Appl. Phys. Lett.* **24** 593
[3] Büttiker M and Landauer R 1982 *Phys. Rev. Lett.* **49** 1739
[4] Haavig D L and Reifenberger R 1982 *Phys. Rev.* B **26** 6408
[5] Truax D R 1982 *J. Math. Phys.* **23** 43
[6] Truscott W S 1993 *Phys. Rev. Lett.* **70** 1900
[7] Stovneng J A and Hauge E H 1989 *J. Stat. Phys.* **57** 841
[8] Hauge E H and Stovneng J A 1989 *Rev. Mod. Phys.* **61** 917
[9] Stovneng J A and Hauge E H 1993 *Phys. Rev.* B **47** 10 446
[10] Azbel M Ya 1992 *Phys. Rev.* B **46** 7596
[11] Stone A D, Azbel M Ya and Lee P A 1985 *Phys. Rev.* B **31** 1707
[12] Jauho A P and Jonson M 1989 *Superlatt. Microstruct.* **6** 303
[13] Jauho A P 1990 *Phys. Rev.* B **41** 12 327
[14] Jauho A P 1992 *Quantum Transport in Semiconductors* (New York: Plenum)
[15] Cai W, Zheng T F, Hu P, Yudanin B and Lax M 1989 *Phys. Rev. Lett.* **63** 418
[16] Cai W, Zheng T F, Hu P, Lax M, Shum K and Alfano R R 1990 *Phys. Rev. Lett.* **65** 104
[17] Jiang X P 1990 *J. Phys.: Condens. Matter* **2** 6553
[18] Wagner M 1994 *Phys. Rev.* B **49** 16 544
[19] Wagner M 1995 *Phys. Rev.* **A51** 798
[20] Sollner T C L G, Goodhue W D, Tannenwald P E, Parker C D and Peck D D 1983 *Appl. Phys. Lett.* **43** 588
[21] Chitta V A, de Bekker R E M, Maan J C, Hawksworth S J, Chamberlain J M, Henini M and Hill G 1992 *Surf. Sci.* **263** 227
[22] Chitta V A, de Bekker R E M., Maan J C, Hawksworth S J, Chamberlain J M, Henini M and Hill G 1992 *Semicond. Sci Technol.* **7** 432
[23] Chitta V A, Kutter C, de Bekker R E M, Maan J C, Hawksworth S J, Chamberlain J M, Henini M and Hill G 1994 *J. Phys.: Condens. Matter* **6** 3945
[24] Dakhnovskii Yu and Metiu H 1995 *Phys. Rev.* B **51** 4193
[25] Liu H C 1991 *Phys. Rev.* B **43** 12 538
[26] Wingreen N S, Jauho A P and Meir Y 1993 *Phys. Rev.* B **48** 8487
[27] Jauho A P, Wingreen N S and Meir Y 1994 *Phys. Rev.* B **50** 5528
[28] Landau L D and Lifshitz E M 1977 *Quantum Mechanics: Non-Relativistic Theory* (New York: Pergamon) pp 173, 174
[29] Johansson P and Wendin G 1992 *Phys. Rev.* B **46** 1451
[30] Iñarrea J, Platero G and Tejedor C 1994 *Phys. Rev.* B **50** 4581
[31] Bonnefoi A R, McGill T C, and Burnham R D 1988 *Phys. Rev.* B **37** 8755
[32] Mendez E E, Calleja E and Wang W I 1986 *Phys. Rev.* B **34** 6026
[33] Ando T, Wakahara S and Akera H 1989 *Phys. Rev.* B **40** 11 609
[34] Björksten M F, Nieminen R M and Laasonen K 1991 *J. Phys.: Condens. Matter* **3** 7007
[35] Brown E R, Sollner T C L G, Parker C D, Goodhue W D and Cheng C L 1989 *Appl. Phys. Lett.* **55** 1777
[36] Garcia-Calderon G 1993 *The Physics of Low-Dimensional Semiconductor Structures* ed Butcher *et al* (New York: Plenum)
[37] Frishman A M and Gurvitz S A 1993 *Phys. Rev.* B **47** 16 348
[38] Berman G P, Bulgakov E N, Campbell D K and Sadreev A F 1994 *Preprint* Los Alamos